THE ASTROPHYSICAL JOURNAL, 351:642–650, 1990 March 10

THE ECLIPSING MILLISECOND PULSAR PSR 1957+20

A. S. FRUCHTER,[1,2] G. BERMAN,[1] G. BOWER,[1] M. CONVERY,[1] W. M. GOSS,[3] T. H. HANKINS,[3,4]
J. R. KLEIN,[1] D. J. NICE,[1] M. F. RYBA,[1] D. R. STINEBRING,[1] J. H. TAYLOR,[1] S. E. THORSETT,[1]
AND J. M. WEISBERG[5]

Received 1989 May 25; accepted 1989 September 12

Observations over the past year have yielded detailed information on the eclipsing millisecond pulsar PSR 1957+20 and its orbiting companion. We have found the pulsar to be similar in many ways to other millisecond pulsars: its spin parameters are extremely stable, its period derivative is very small ($1.61 \pm 0.09 \times 10^{-20}$), its profile has a strong interpulse, and its radio spectrum has a steep power-law index of about -3. The orbit is nearly circular, with an eccentricity less than 2×10^{-5}, and the mass function implies a companion mass not much greater than 0.022 $M_\odot$. Eclipses last for approximately 56 and 50 minutes at 318 and 430 MHz, respectively, corresponding to a $\nu^{-0.41 \pm 0.09}$ dependence of eclipse duration on frequency, at least over this small range. Excess delays of the pulsed signal near the edges of eclipse depend on frequency approximately as ν^{-2} and vary substantially from one eclipse to another. The average pulse profile shows weak circular and almost no linear polarization. An absence of measurable Faraday delays between left and right circularly polarized components implies that the mean longitudinal magnetic field is no more than a few gauss in the region just outside the eclipsing material.

The available evidence points strongly toward a system in which radiation from the pulsar heats the companion to the point of ablation, thereby driving a stellar wind that trails outward and behind the companion, somewhat like a comet tail. The lack of measurable change in the orbital period of the system suggests a time scale for evaporation of the companion greater than 10^7 yr.

Subject headings: pulsars — stars: eclipsing binaries — stars: evolution — stars: individual (PSR 1957+20)

I. INTRODUCTION

Of the nine well-documented examples of radio pulsars in binary systems, PSR 1957+20 is the only one regularly eclipsed by its companion star. At 1.607 ms, the pulsar period is second fastest among all currently known pulsars, and the orbital period of 9.17 hr is the second shortest in the group. The discovery and immediate follow-up observations (Fruchter, Stinebring, and Taylor 1988) showed that (1) the pulsar disappears in eclipses behind the companion star for nearly 10% of each orbit, (2) the companion's mass is approximately 0.025 $M_\odot$, and (3) the Roche lobe of the companion is much smaller than the eclipsing region, indicating that gas from the companion's atmosphere must continuously replenish the eclipsing medium. The surprising implication is that we are witnessing the evaporation of the companion star by radiation from the pulsar. Remarkably, behavior of this kind had been foreseen in a paper by Ruderman, Shaham, and Tavani (1989). Some astrophysical consequences of the early observations have been discussed by Kluźniak *et al.* (1988), Michel (1989), Phinney *et al.* (1988), Rasio, Shapiro, and Teukolsky (1989), van den Heuvel and van Paradijs (1988), and others.

We have continued to make regular observations of PSR 1957+20, and further details are now available concerning the pulse profile, spectrum, polarization, orbit, and propagation phenomena surrounding eclipses. In this paper we elaborate upon the brief summaries given by Stinebring *et al.* (1989) and Thorsett *et al.* (1989) and present observations beyond those described in Fruchter (1989). In § II we describe how the observations were accomplished, and in §§ III–V we report the principal results. Some inferences and conclusions are presented in § VI.

II. OBSERVATIONS

The very short period, moderately large dispersion measure, low flux density, and unusually steep spectrum of PSR 1957+20 conspire to make it a difficult and challenging pulsar to observe. For these reasons, nearly all of our observations have been made with the 305 m telescope of the Arecibo Observatory,[6] where the pulsar was discovered, and with the benefit of coherent dedispersing radiometers that we have built over the past several years (Hankins, Stinebring, and Rawley 1987; Ryba 1988). Successful observations have now been made of the pulsar at frequencies near 318, 430, 606, and 1400 MHz, though most of the data with high signal-to-noise ratios were obtained at either 318 or 430 MHz. Parameters of the Arecibo telescope and the relevant receiving equipment are listed in Table 1, together with the approximate number of hours that we have observed with each system.

In the three lowest frequency bands, all observations after the initial discovery and confirmation were made using real-time coherent dispersion removal (see Hankins and Rickett 1975 for a discussion of this technique). The dedispersing hardware is based on charge-coupled devices (CCDs) manufactured by EG&G Reticon. With appropriate supporting circuitry, each model RT5601A-2 chip carries out a 512 lag convolution with a "chirp" kernel that rotates signal phases so as to mimic (in reverse) the dispersive effect of the interstellar medium. The

[1] Joseph Henry Laboratories and Physics Department, Princeton University.
[2] Department of Terrestrial Magnetism, Carnegie Institution of Washington.
[3] National Radio Astronomy Observatory, Socorro, New Mexico.
[4] Department of Physics and Astronomy, New Mexico Institute of Mining and Technology.
[5] Department of Physics and Astronomy, Carleton College.

[6] The Arecibo Observatory is part of the National Astronomy and Ionosphere Center, operated by Cornell University under contract with the National Science Foundation.

TABLE 1

PARAMETERS OF THE OBSERVING SYSTEMS

Frequency (MHz)	Maximum Sensitivity (K Jy^{-1})	System Temperature (K)	Front End Bandwidth (MHz)	Polarizations	Detected Bandwidth (MHz)	Observing Time (hr)
318.....	6.5	300	18	1 L	2 × 0.26	9
430.....	18	170	10	2 C	2 × 0.41	29
606.....	5.5	120	10	1 L	2 × 0.69	2
1408.....	7.5	40	40	2 C	32 × 0.25	3

dispersive delay at frequency v is $t = D/v^2$, where D is the "dispersion constant," conventionally related to the dispersion measure by DM $= (2.41 \times 10^{-16})D$, with DM in units of cm^{-3} pc. With a fixed number N of lags in the discrete convolution, the frequency v_c of a clock signal driving the CCD depends on the dispersion sweep rate, $\alpha = dv/dt$, and in turn determines the maximum usable bandwidth, Δv, through the relation

$$\Delta v = \tfrac{1}{2}v_c = \tfrac{1}{2}(N\alpha)^{1/2} = 7.855 v_{\rm GHz}^{1.5}(\rm DM)^{-0.5}\,, \qquad (1)$$

where Δv is in MHz, $v_{\rm GHz}$ is the observing frequency in GHz, and in our implementation $N = 512$. For PSR 1957+20, with DM ≈ 29.1 cm^{-3} pc, the usable bandwidths for our lowest three observing frequencies range from 0.26 to 0.69 MHz per dedispersed channel, as indicated in the sixth column of Table 1.

For most of these observations, two copies of the coherent dedispersing circuitry were available. Thus, two independent dedispersed signals could be detected in square-law detectors, measuring the intensities of a single polarization in each of two passbands separated by less than the bandwidth of the receiver front end and feed system. Alternatively, at 430 MHz the dual–circularly polarized feed permitted recording the intensities of two orthogonal polarizations at the same frequency, or, with the use of a multiplying polarimeter constructed for this purpose (Thorsett 1989), measuring the full Stokes parameters of the received signal. Each of these modes of operation was used for some of the observations.

Single pulses from PSR 1957+20 are much too weak to be detected, even with the high sensitivity of the Arecibo antenna. Consequently, after coherent dispersion removal and square-law detection, the received signals were smoothed with a time constant of 6 μs, sampled at 1024 samples per period, and averaged synchronously for intervals ranging from 10 to 60 s. This was accomplished with the "Mark III" data acquisition system that we have developed for use in high-precision pulsar timing observations (Hankins and Stinebring 1990; Berman 1989; see also Taylor and Weisberg 1989 for some early results with this system). The data acquisition hardware maintains phase with a pulsar by adjusting, once per second, the frequency of a clock signal generated by a continuous-phase digital synthesizer. The clock frequencies are determined by evaluating a high-order polynomial whose coefficients have been calculated in advance, using a tabulated ephemeris of Earth's motion and the best currently available spin and orbital parameters for the pulsar.

Our 1408 MHz observations of PSR 1957+20 at Arecibo have been made with postdetection dispersion compensation, the signal averager recording sums of detected signals from orthogonal polarizations in 32 0.25 MHz channels and 32 0.625 MHz channels. For these observations we used postdetection time constants of 10 and 40 μs, respectively, and the accumulated average profiles had only 128 phase bins.

Much of the interesting information obtained on the PSR 1957+20 system comes from measurement and analysis of its pulse times of arrival, or TOAs. The procedures are identical to those currently being used for other fast pulsars (e.g., Rawley, Taylor, and Davis 1988; Taylor and Weisberg 1989). Each integrated pulse profile is tagged with the time of the first sample in a period close to the midpoint of the integration. The profile is matched with a high signal-to-noise ratio "standard profile" to determine the pulse phase by a least-squares procedure. A time delay corresponding to the measured phase is added to the start time to yield the topocentric TOA.

III. CHARACTERISTICS OF THE PULSAR

Samples of the integrated pulse waveforms of PSR 1957+20 at four frequencies are presented in Figure 1. At 430 MHz, where the signal-to-noise ratio is highest, the profile consists of a narrow main pulse, 35 μs wide at half-intensity points, and a broad, asymmetric interpulse. The interpulse extends over some 380 μs, or 0.24 of the period, centered almost exactly half a period away from the peak of the main pulse. The main pulse/interpulse nomenclature is actually rather arbitrary; with the terminology we are using, approximately 56% of the flux density comes from the interpulse at 430 MHz. Weak, marginally significant pulse components appear to be present in the 430 MHz profile about 0.20 of a period before the peaks of both main pulse and interpulse. Both of these features are also marginally visible in the 606 MHz profile, and at 1408 MHz the one preceding the interpulse is nearly as strong as the main pulse. Obviously the spectrum of this component falls off much less steeply than the rest. High signal-to-noise ratio

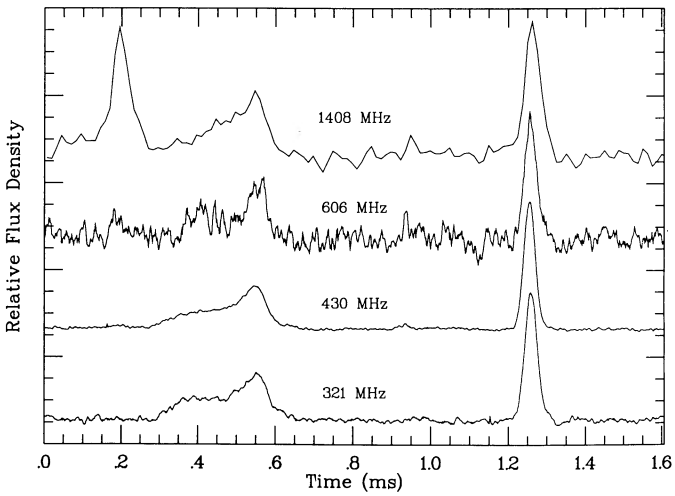

FIG. 1.—Average profiles of PSR 1957+20 at 321, 430, 606, and 1408 MHz. Instrumental time constants were approximately 6 μs at the three lower frequencies and 10 μs at 1408 MHz.

observations may reveal further interesting dependences of pulse shape on frequency.

Like other pulsars with dispersion measures less than several hundred cm^{-3} pc, PSR 1957+20 exhibits strong diffractive scintillations in the frequency range of our observations. Averaged over the detected bandwidths of 0.26 MHz at 318 MHz and 0.41 MHz at 430 MHz, the observed flux density of the pulsar varies by a factor of 10 or more on time scales of a few minutes. Individual profiles have been recorded with signal-to-noise ratios as high as S/N = 100 in 1 minute integrations, though values of 10–20 are more typical. Occasional scintillation minima have been seen in which the signal disappeared entirely (S/N < 3) for up to 5 minutes. When two received channels were offset by 5 MHz or more around either 318 or 430 MHz, scintillations in the two channels appeared to be completely uncorrelated. Estimates of the pulsar's time-averaged flux densities at 318, 430, and 606 MHz, scaled from the observed profiles by using the known dependence of system noise temperature and antenna gain on zenith angle, are plotted in Figure 2.

VLA[7] observations were made in C array on 1988 April 4 and 13 and showed the pulsar to have a flux density of 0.35 ± 0.15 mJy in a 100 MHz bandwidth centered at 1490 MHz. This measurement is plotted in Figure 2 together with those made at lower frequencies at Arecibo, clearly documenting the steepness of the pulsar spectrum and its power-law index close to -3. The VLA observations also provided a position measurement, $\alpha = 19^h57^m24^s.9 \pm 0^s.1$, $\delta = 20°39'58'' \pm 2''$ (B1950.0), which greatly facilitated our early timing work as well as optical identification of the pulsar's companion (Kulkarni, Djorgovski, and Fruchter 1988; Fruchter *et al.* 1988).

Observations at 430 MHz using the multiplying polarimeter on the coherently dedispersed signal yielded the results shown in Figure 3. All of these measurements were made at phases well away from eclipse. The polarimeter was calibrated by observing the unpolarized reference source 3C 410, and system integrity was further verified with observations of the millisecond pulsar PSR 1937+21. Results for the latter source were in good agreement with previously published data (Stinebring and Cordes 1983). As shown in Figure 3, linear polarization amounts to no more than 3% in the PSR 1957+20 profile, while circular polarization reaches a maximum of about 10% and changes sign near the middle of both main pulse and interpulse. We have not made polarization measurements at any other frequencies.

[7] The Very Large Array telescope is part of the National Radio Astronomy Observatory, operated by Associated Universities, Inc., under contract with the National Science Foundation.

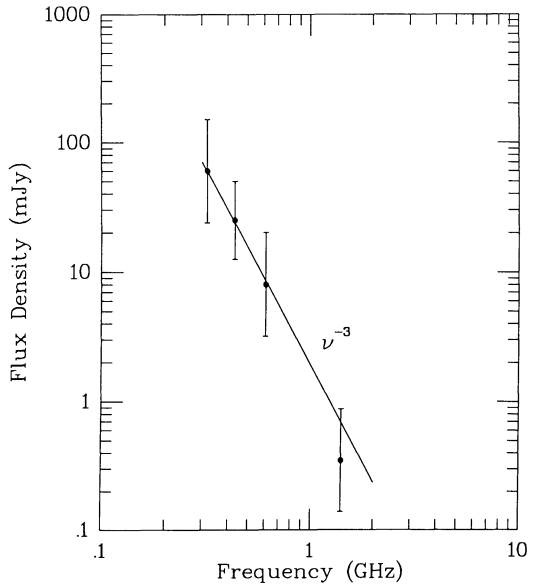

FIG. 2.—Radio frequency spectrum of PSR 1957+20 from 318 MHz to 1480 MHz.

IV. ANALYSIS OF TIMING DATA

A total of 4011 pulse times of arrival were measured between 1988 March 24 and 1989 March 1. The topocentric TOAs were corrected to the solar system barycenter and standard techniques used to obtain least-squares estimates of the astrometric, dispersion, spin, and orbital parameters listed in Table 2.

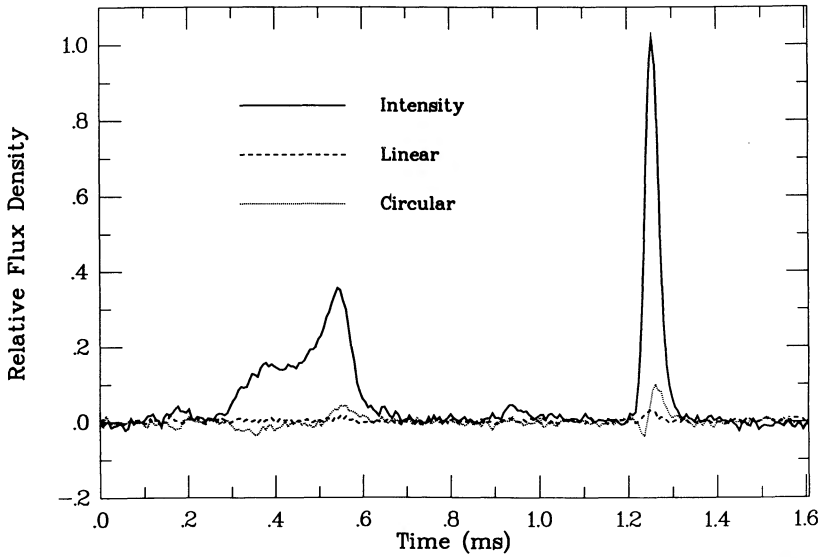

FIG. 3.—Total intensity, linearly polarized component, and circular component of pulsed emission from PSR 1957+20 at 430 MHz

TABLE 2

PARAMETERS OF THE PSR 1957+20 SYSTEM[a]

Parameter	Value
Right ascension (B1950)	$19^h57^m24^s.9926(5)$
Right ascension (J2000)	$19^h59^m36^s.7729(5)$
Declination (B1950)	$20°39'59''.817(9)$
Declination (J2000)	$20°48'15''.163(9)$
Dispersion measure (cm^{-3} pc)	29.117(2)
Period (ms)	1.6074016836502(8)
Period derivative (10^{-20})	1.61 ± 0.09
Epoch (JED)	2,447,402.0700
Projected semimajor axis (lt = s)	0.0892267(15)
Orbital period (s)	33001.9167(4)
Time of ascending node (JED)	2,447,402.0729653(12)
Eccentricity	$<2 \times 10^{-5}$
Orbital period derivative	$(0.4 \pm 1.0) \times 10^{-10}$

[a] Figures in parentheses are uncertainties in the last digit quoted. B1950 positions are in the coordinate system of the Center for Astrophysics PEP740R ephemeris; J2000 positions refer to the JPL DE200 ephemeris.

Some details of the necessary procedures may be found in Manchester and Taylor (1977) and Taylor and Weisberg (1989). Notable among the measured parameters is the period derivative, $\dot{P} = (1.61 \pm 0.09) \times 10^{-20}$, the smallest spin-down rate known for any pulsar. In the upper portion of Figure 4, we illustrate the orbital solution by plotting the 4011 measurements of signal delay caused by motion of the pulsar relative to the system barycenter. In this figure and elsewhere in this paper, orbital phases are measured from the time of ascending node.

At low frequencies the pulsar is totally eclipsed between orbital phases approximately 0.2 and 0.3. Although the effects are too small to be seen in the top panel of Figure 4, observations yield TOAs significantly later than those predicted from the orbital model for phases between 0.195 and signal disappearance, and between reappearance and orbital phase 0.36. As described below, propagation effects rather than dynamical causes are believed to be responsible. Therefore, the TOAs for orbital phases 0.19–0.38 have been given zero weight in the timing solution. Residuals for all of the measured TOAs, including those assigned zero weight, are plotted in the lower portion of Figure 4 with the vertical scale expanded nearly 200 times. Except for phases near eclipse, the observations agree extremely well with the model.

Just three orbital parameters—the projected semimajor axis of the pulsar's orbit, $a_1 \sin i$; the orbital period, P_b; and the time of ascending node—are needed to describe the observations to the full accuracy demanded by the data. (The angle i is the inclination between the plane of the orbit and the plane of the sky.) Because of their potential astrophysical interest, we have also determined upper limits for orbital eccentricity, e, and orbital period derivative, $\dot{P}_b$, and we list these limits at the bottom of Table 2. The physical significance of $\dot{P}_b$ is discussed in § VI.

Previous observations of the millisecond pulsars 1855+09, 1937+21, and 1953+29 (Rawley *et al.* 1987; Rawley, Taylor, and Davis 1988) have shown their long-term rotational stabilities to be extremely high. Our present observations show the same to be true of PSR 1957+20. After excluding the data around eclipse and reducing the data to a single equivalent TOA for each observing frequency on each day, we obtain a postfit root-mean-square residual of approximately 1.5 μs. As illustrated in the daily average residual plot of Figure 5, there are no significant indications of timing noise or other unmodeled effects contributing more than a few microseconds to the TOAs.

V. PHENOMENA SURROUNDING ECLIPSES

The characteristic that distinguishes PSR 1957+20 from all other known radio pulsars is its eclipse, lasting approximately 10% of the orbital period and centered one-quarter of a period after the time of ascending node. The gray-scale plot of Figure 6 illustrates reappearance of the pulsar signal from an eclipse on 1988 June 26, at a time when the pulsar was unusually strong at 430 MHz and could be seen in 10 s integrations. No signal is visible from the beginning of the record until orbital phase $\phi \approx 0.298$, when the main pulse reappears near the bottom of the figure and almost immediately wraps around to the top. The phase reference for the vertical scale of the figure is such that orbital motion of both the pulsar and Earth have

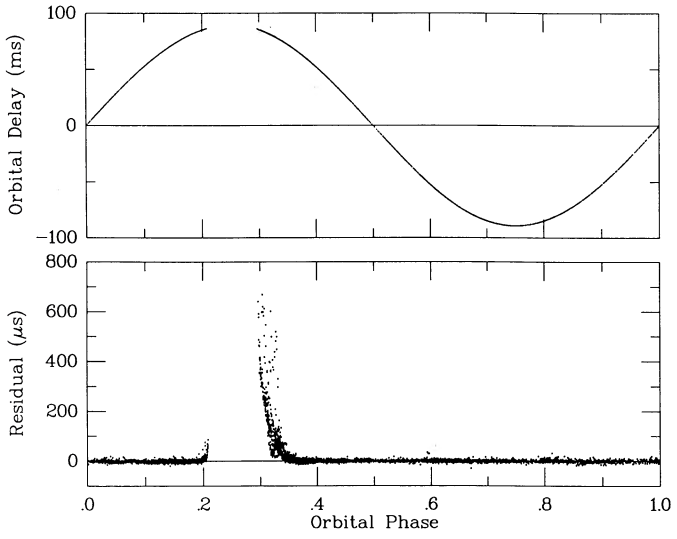

FIG. 4.—*Top*: delays of pulse arrival times caused by orbital motion of PSR 1957+20 about the system barycenter. A total of 4011 individual points blend together to form a nearly continuous curve. The pulsar is eclipsed between phases of approximately 0.207 and 0.297. *Bottom*: arrival time residuals after subtracting the model whose parameters are listed in Table 2.

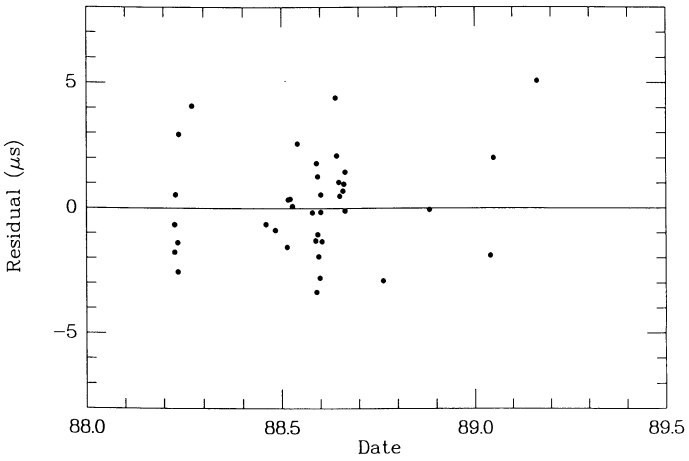

FIG. 5.—Residuals for daily average pulse arrival times relative to the model in Table 2. Observations at orbital phases 0.19–0.38 were not included in the averages.

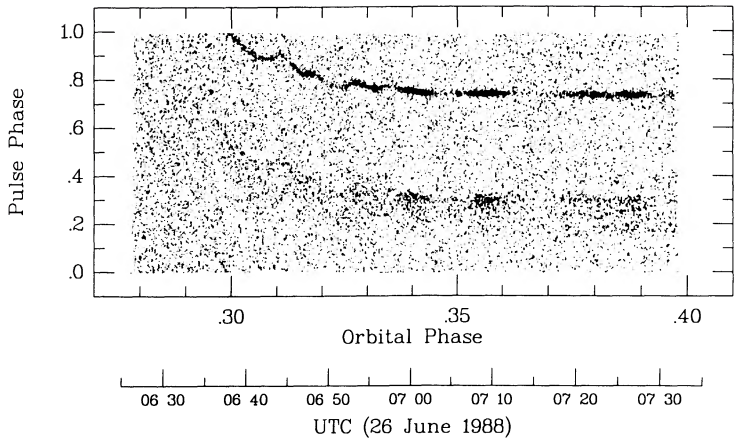

FIG. 6.—Observed signal strength as a function of orbital phase and pulsar phase, for a 66 minute interval on 1988 June 26. Darker regions correspond to stronger signals. The pulsar emerges from eclipse at orbital phase 0.298. The broad interpulse can be seen in the lower portion of the figure, especially around orbital phase 0.35.

been accounted for; in the absence of unmodeled propagation effects, the narrow main pulse should remain at pulse phase 0.73. Instead, the pulse is seen to drift gradually (though not monotonically) from 1.05 down to 0.73 over some 30 minutes. The typical scintillation time scale of ~ 5 minutes can also be seen in Figure 6, as can a nearly complete scintillation fade-out lasting for about 5 minutes near $\phi \approx 0.365$.

A total of 12 eclipse disappearances and reappearances have been observed at 318 and 430 MHz, in addition to seven "near misses" in which the critical events occurred close to or just outside the telescope's zenith angle limit. Mean values and standard deviations of the observed orbital phases at disappearance and reappearance are listed in Table 3, with separate entries for 318 and 430 MHz. From this information the eclipse duration, listed in the last column of the table, is found to be 6.6 ± 1.5 minutes longer at the lower frequency. By assuming a power-law dependence of eclipse duration on frequency, we obtain -0.41 ± 0.09 for the frequency exponent over the narrow range 318 to 430 MHz.

A single eclipse disappearance has been observed at 1408 MHz. It occurred at $\phi = 0.223 \pm 0.005$, well inside the lower frequency eclipse points and consistent with the empirical $\nu^{-0.4}$ scaling law for eclipse duration. Further observations of phenomena surrounding the eclipses will be carried out soon at 1400 MHz and higher frequencies.

The excess pre- and post-eclipse delays seen in the residuals of Figure 4 are replotted with higher resolution in Figure 7. The 430 and 318 MHz data are plotted separately and different symbols are used for different observing days, so that one may follow variations in propagation delay as they evolved. We emphasize that bandwidth limitations of the Arecibo telescope prevent the observation of a particular eclipse at both frequencies, so frequency-dependent behavior must be inferred from an ensemble of eclipses. At ingress the maximum delay we have seen is about 100 μs, with all excess occurring within about 6 minutes of eclipse entrance (left side of Fig. 7). In contrast, the initial delays following egress are around 500 μs at both 318 MHz and 430 MHz, and subsequent values take 30 or 35 minutes to decrease asymptotically toward zero (right side of Fig. 7). During the half-hour after eclipse, substantial variations are often seen—including, on several occasions at 318 MHz, secondary enhancements almost as big as the initial delay at reappearance. In our limited experience, the day-to-day variations have been larger at 318 than at 430 MHz.

Despite the considerable differences among the curves shown in Figure 7, the data are consistent with propagation delays that scale with observing frequency as ν^{-2}, as expected from the cold plasma dispersion relation. A more quantitative measure of the frequency dependence is provided by observations made simultaneously at 312 and 327 MHz for an eclipse ending at 0444 UT on 1988 July 19. The measured excess delays at these two frequencies are plotted against each other in Figure 8. The best-fitting straight line has the equation

$$\Delta t_{312} = (1.09 \pm 0.01)\Delta t_{327} , \quad (2)$$

which corresponds to a power-law relation

$$\Delta t_{\nu} \propto \nu^{-1.8 \pm 0.2} \quad (3)$$

for the excess delays and confirms that the responsible mechanism is probably dispersion in an ionized medium.

While the post-eclipse delays are significantly larger and longer lasting than the pre-eclipse delays, the eclipse itself is nearly centered on orbit phase 0.25 (see Table 3), as expected from a symmetric eclipsing body. Any viable model for this system must explain both the asymmetry of the pre- and post-eclipse delays, and the symmetry of the eclipse.

It is well known that the indices of refraction for left and right circularly polarized waves in an ionized medium differ in

TABLE 3

ECLIPSE DISAPPEARANCES AND REAPPEARANCES AT 318 AND 430 MHz

FREQUENCY (MHz)	DISAPPEARANCES		REAPPEARANCES		DURATION (minutes)
	Number	Phase	Number	Phase	
318.....	3	0.2011 ± 0.0015	3	0.3038 ± 0.0015	56.5 ± 1.2
430.....	3	0.2068 ± 0.0012	3	0.2975 ± 0.0010	49.9 ± 0.9

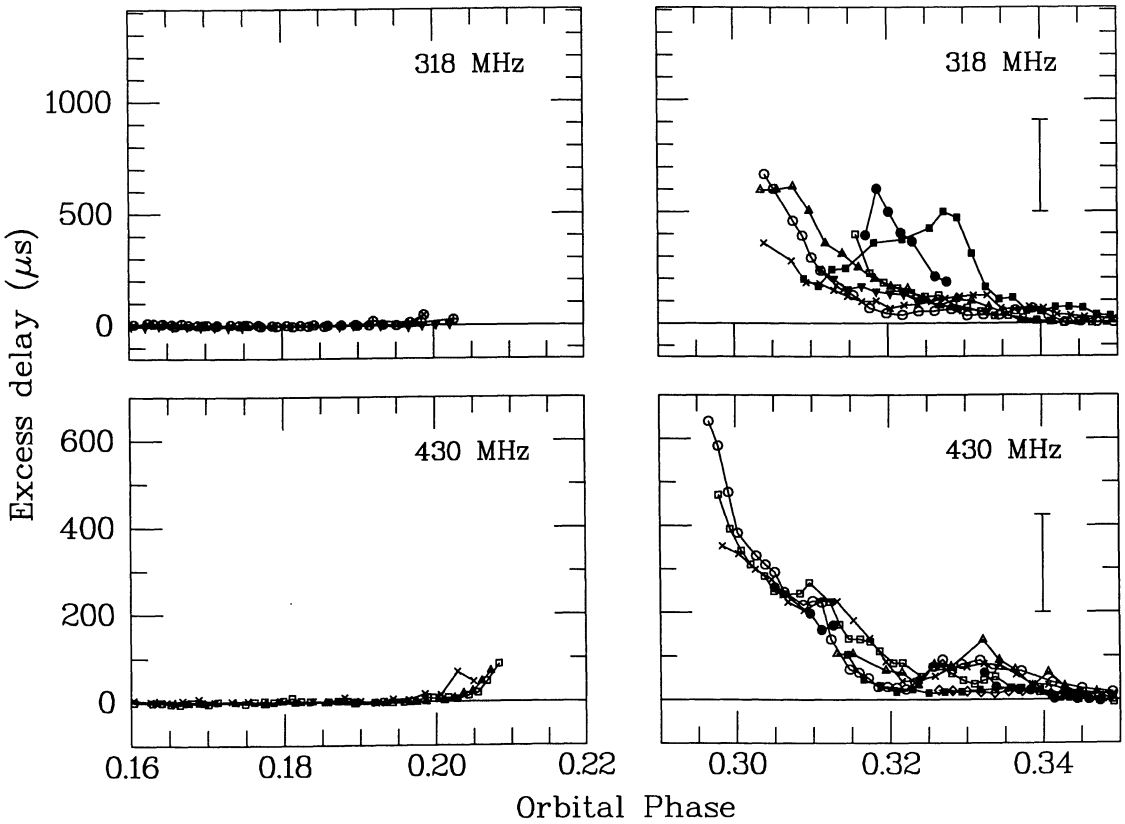

FIG. 7.—Pre- and post-eclipse excess propagation delays observed at 318 MHz (*top*) and 430 MHz (*bottom*). Different symbols correspond to different observing days at each frequency. Due to bandwidth limitations of the Arecibo telescope, no single eclipse has been observed at both frequencies. The vertical scales for data at the two frequencies are different by a factor of $(430/318)^2 = 1.83$. The effect of an incremental dispersion contribution of $\Delta DM = 0.01$ cm^{-3} pc is indicated by the vertical bars.

the presence of a parallel magnetic field. The resulting Faraday time delay between the arrival of the two polarizations is given by the relation

$$\Delta t_F = \frac{e \Delta t_\nu B_\parallel}{2\pi mc\nu}, \quad (4)$$

where e and m are the electron charge and mass, c is the speed of light, Δt_ν is the excess dispersive time delay at frequency ν, and

$$B_\parallel = \frac{\int n_e \boldsymbol{B} \cdot \boldsymbol{dl}}{\int n_e dl} \quad (5)$$

is the average longitudinal component of the magnetic field in the region of the eclipse, weighted by electron density. At our observing frequency of 430 MHz, this equation implies $B_\parallel = 38.4\,\Delta t_F/\Delta t_\nu$ gauss.

We have made circular polarization observations of three eclipses at 430 MHz in an attempt to measure a differential Faraday delay between the left and right circularly polarized signals. The results are plotted as constraints on $B_\parallel$ in Figure 9. Because the fractional uncertainties in Δt_ν are much smaller than those in Δt_F, the latter dominate, with the fortuitous consequence that the uncertainties in $B_\parallel$ are smallest in the regions of large Δt_ν near eclipse. At a 95% confidence level, we find an average parallel magnetic field $B_\parallel = -1.5 \pm 4.5$ and 0.4 ± 1.0 G before and after eclipse, respectively. In the 10 minutes after reappearance, where $\Delta t_\nu > 100$ μs, $B_\parallel = 0.1 \pm 0.5$ G. Stronger fields which change sign either temporally or spatially along the line of sight are allowed, as are field components perpendicular to the line of sight. Any model of the eclipsing region that requires large magnetic fields will need to explain in a natural way how such complete cancellation is achieved.

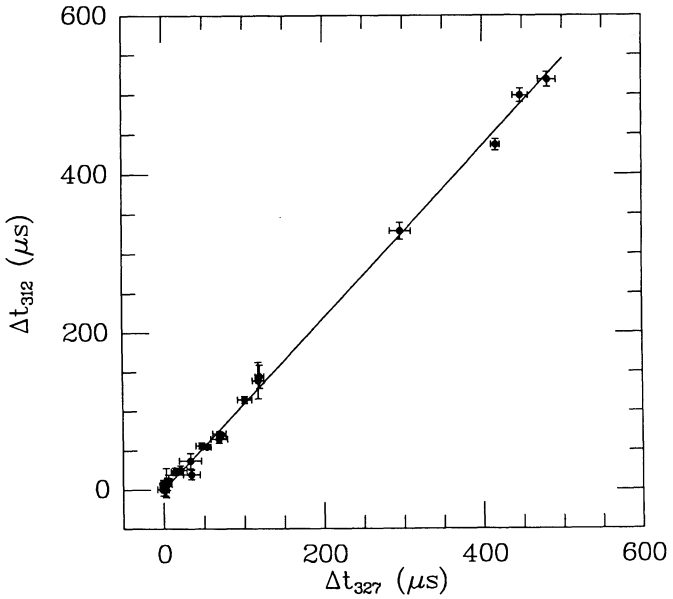

FIG. 8.—Excess group delays observed in simultaneous measurements at 312 and 327 MHz on 1988 July 19. The best-fitting straight line has a slope of 1.09 ± 0.01, which corresponds to a frequency dependence $\Delta t_\nu \propto \nu^{-1.8 \pm 0.2}$.

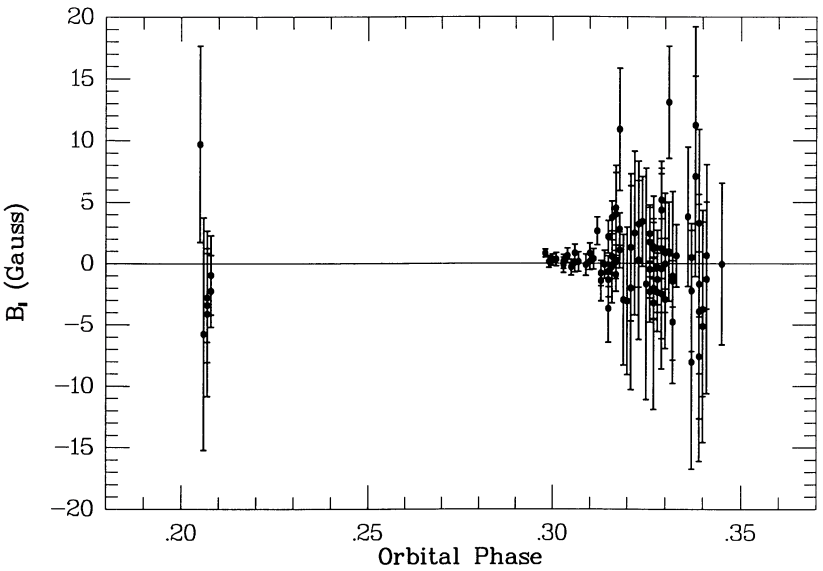

FIG. 9.—Measured values of average parallel magnetic field from Faraday delay measurements, plotted wherever the excess dispersive delay Δt_v exceeds 20 μs

VI. DISCUSSION AND CONCLUSIONS

In this section we review earlier observations of the eclipsing binary pulsar, discuss the new observations presented in this paper, and investigate the implications of these observations for several models proposed to explain the eclipse. The PSR 1957+20 system consists of a neutron star, assumed to have mass $m_1 \approx 1.4\ M_\odot$, and a companion of mass $m_2 \approx 0.022\ M_\odot/\sin i$ separated by orbital radius $a \approx 2.4\ R_\odot$ (Fruchter, Stinebring, and Taylor 1988). The pulsar is eclipsed by its companion for nearly 10% of the orbit, implying a half-width of the eclipsing region, $R_E \approx 0.75\ R_\odot$. The eclipse suggests we are viewing the system nearly edge-on; therefore sin i is near unity, and the companion mass is almost certainly less than $0.04\ M_\odot$. Most of the eclipsing material then lies outside the companion's Roche lobe ($R_L \approx 0.3\ R_\odot$), and must therefore be constantly replenished by a stellar wind from its surface. The excess delay of the pulsar signal shortly before ingress and for many minutes after egress is due to passage of the signal through the companion's stellar wind. The disparity in delay times at eclipse entrance and exit suggests the presence of a cometary tail swept back by the orbital motion.

The measured pulsar period and period derivative imply a spin-down energy loss rate $\dot{E} = 4\pi^2 I \dot{P} P^{-3} \approx 40\ L_\odot$, where we have assumed a moment of inertia $I \approx 10^{45}$ g cm^2. If this energy is radiated isotropically, then the energy flux at the distance of the companion is $40\ L_\odot/(4\pi a^2)$, or about 7 times greater than that at the surface of the Sun. This energy not only drives the eclipsing stellar wind, but also heats the side of the companion facing the pulsar to at least several thousand K, making it optically visible (Kulkarni, Djorgovski, and Fruchter 1988; Fruchter *et al.* 1988; van Paradijs *et al.* 1988; Djorgovski and Evans 1988). The light from the companion varies by more than 3 mag as the side illuminated by the pulsar becomes more or less visible from Earth. The maximum optical luminosity suggests a companion size $R_2 = 0.1$–$0.15\ R_\odot$, agreeing with the theoretical value for the radius of a degenerate hydrogen dwarf of mass $\approx 0.02\ M_\odot$. Thus the optical observations confirm that the energy source for the eclipsing wind is indeed the pulsar, and require the size hierarchy $R_2 < R_L < R_E$.

Measurement of the companion's color temperature and the pulsar's period derivative allow us to place limits on the fraction f of spin-down energy reaching the companion's photosphere. Using, as above, the standard estimates of neutron star mass and moment of inertia, and assuming that the spin-down energy is radiated isotropically, we find, following Fruchter *et al.* (1988), that

$$f = (0.27 \pm 0.06)\left(\frac{T_2}{5750\ \mathrm{K}}\right)^4, \tag{6}$$

where T_2 is the surface temperature of the companion. Unfortunately, the uncertainty in T_2 is at least 500 K because of uncertainties in interstellar reddening and temperature distribution over the surface of the companion (Fruchter 1989). Moreover, although Fruchter *et al.* (1988) argue that the reddening is $A_V = 1.5$, if the true value is as high as $A_V = 3.0$, as could be inferred by the unusual Balmer decrement of the Hα nebula about the pulsar (Kulkarni and Hester 1988), the surface temperature of the companion could be as high as 8000 K. This temperature would require that essentially all of the pulsar spin-down energy directed at the companion reaches the photosphere. Direct measurements of interstellar reddening in this region of sky would improve our understanding of the energetics of the PSR 1957+20 system and allow tighter constraints to be placed on the energy available to fuel an evaporative wind.

The timing observations also allow us to place a limit on the rate of change of the orbital period, and indirectly on the rate of evaporation of the companion. Let the constant β represent the ratio of specific angular momentum of the evaporating mass to that of the companion star. It can be shown (see Czerny and King 1988) that

$$\frac{\dot{P}_b}{P_b} = \frac{3(\beta - 1)\dot{m}_2}{m_2} + \frac{(1 - 3\beta)\dot{m}_2}{m_1 + m_2}. \tag{7}$$

Unless β is nearly unity, the time scales for orbital period evolution and evaporation of the companion will be comparable. Therefore our upper limit on $|\dot{P}_b|$ suggests that the time scale for evaporation probably exceeds 10^7 yr. While this limit does not place serious constraints on most models of the

system, we note that with continued timing measurements the uncertainty in $\dot{P}_b$ should decrease as the inverse square of the data span (currently about 1 year). Within a decade, very interesting constraints on the orbital decay time scale should be available.

At least three classes of model have been proposed to explain the pulsar eclipse and the associated pre- and post-eclipse delays. Phinney *et al.* (1988) and Kluźniak *et al.* (1988) suggest that the eclipse is due to reflection or refraction of the pulsar's signal by a dense plasma contained behind a contact discontinuity. Wasserman and Cordes (1988) and Rasio, Shapiro, and Teukolsky (1989) model the eclipse as free-free absorption in a plasma streaming off the companion; and Michel (1989) proposes that the eclipsing material is largely confined within the companion's magnetosphere. Here we compare the predictions of these models with the observations.

In the model of Phinney *et al.* (1988) and Kluźniak *et al.* (1988), the eclipse is caused by an overdense plasma contained behind a contact discontinuity, and the excess propagation delays seen immediately before and after eclipse are due to the signal's passage through a tenuous plasma surrounding the eclipsing medium. Because refraction or reflection would occur at the rather sharp boundary of the discontinuity, this model does not predict significant dependence of eclipse duration on observing frequency—in contradiction to the simplest interpretation of our results.

All of the observations made at Arecibo, however, have been sensitive only to *pulsed* flux from PSR 1957+20. If propagation effects in the gas surrounding the companion contrive to smear the pulse by a substantial fraction of the pulse period, the pulsed signal would appear to be eclipsed even if the full mean flux density were still present. While the variations in excess propagation delay depicted in Figure 7 seldom contribute more than about 100 μs to pulse broadening in our typical integrations, the onset of additional smearing very close to ingress and egress could be quite sudden. Indeed it seems possible, if not likely, that the column density of dispersing plasma may vary sufficiently rapidly that the eclipse is caused by pulse smearing. Interferometric observations at various frequencies and at orbital phases before, during, and after eclipse could distinguish between the loss of mean flux and an eclipse due to pulse smearing. Such observations are being undertaken at the VLA.

The proposal by Wasserman and Cordes (1988) and Rasio, Shapiro, and Teukolsky (1989) that the eclipse is caused by free-free absorption requires that the plasma surrounding the companion be surprisingly cold, about 300 K. If orbital motion is neglected, the model predicts a dependence of eclipse length upon observing frequency of $\nu^{-2/3}$ for an isothermal companion wind. If the wind cools as it expands, the frequency dependence is much steeper; an adiabatically cooling wind would show an eclipse length dependence of ν^{-2}. However, a wind heated by radiation from the pulsar could perhaps display the relatively shallow frequency dependence that is observed.

By accounting for orbital motion and simulating particle trajectories for the companion wind, Rasio, Shapiro, and Teukolsky (1989) were able to reproduce the asymmetry in the pre- and post-eclipse delays. The ejected particles must leave the companion with a velocity about 10 times the orbital velocity, which leads to the principal difficulty of the model: it requires careful tuning of the behavior of the escaping gas. After leaving the 6000 K surface of the companion, the gas must cool to 300 K in the tail, while at the same time accelerating to a bulk velocity (about 3000 km s^{-1}) corresponding to a kinetic temperature of 10^6 K. While cold, high-velocity flows are not impossible, the lack of a proposed mechanism for powering the flow is a problem.

The success of Rasio, Shapiro, and Teukolsky in reproducing the observed delays suggests that even if free-free absorption proves not to be the correct eclipsing mechanism, their particle trajectory simulations may yield a good approximation to the shape of the companion's wind. In this case, the apparent eclipse could be the result of pulse smearing in the time-varying plasma column density. One can show that in such a model the observed excess delays are in reasonable accord with the observed frequency dependence of eclipse duration. Nonetheless, we find pulse smearing unconvincing as an explanation of eclipse, both because the observed rate of change of delay does not appear to be high enough (see Fig. 7) and because the eclipse is nearly symmetric about $\phi = 0.25$ in spite of the extreme asymmetry of the delays.

Michel's (1989) model of an eclipse caused by a dense plasma contained in the companion's magnetosphere provides a natural explanation of the symmetry of eclipse. He suggests that the tenuous plasma observed shortly before and after eclipse is in the magnetotail, where the magnetic field lines are swept back by the pulsar wind. However, the spin-down luminosity of the pulsar, 40 $L_\odot$, implies a pulsar wind energy density near the companion of about 14 ergs cm^{-3}. If a substantial fraction of this energy is transported by electromagnetic waves or charged particles, the companion's magnetic field at the boundary of the eclipsing medium would have to be approximately 10 G to balance the pulsar wind. For such a field to remain undetected by our Faraday delay measurement would require either that the field be nearly normal to the line of sight or that most of the observed excess column density be provided by electrons at least a few eclipse radii from the companion. While it seems plausible that closed field lines could be nearly orthogonal to the line of sight at eclipse edge, open field lines will tend to follow the plasma and should therefore stream away from the pulsar and toward us. If Michel's model is correct the cometary tail must be well collimated, and the line-of-sight electron density n_e must be small where the parallel component of **B** is large. These conditions seem rather unlikely; moreover, we do not see a natural way to make Michel's magnetospheric model agree with our observations of the frequency dependence of eclipse duration, for his model appears to rely upon a dense plasma to reflect or refract the pulsar signal. If interaction of the plasma with the magnetic field is responsible for the eclipse through cyclotron absorption, one would expect the eclipse duration to scale as $\nu^{-1/3}$, in reasonably good agreement with our results. However, cyclotron absorption appears to require a magnetic field even larger than that necessary to support the pulsar wind (A. C. Thompson, personal communication), and is therefore difficult to reconcile with our limits on the magnetic field.

In this paper we have presented new measurements of the spin and orbital parameters of PSR 1957+20, as well as detailed studies involving the plasma ablated from its companion. We have shown that a substantial fraction of the pulsar's spin-down luminosity reaches the photosphere of the companion; that the plasma surrounding the eclipsing region is not likely to be highly magnetized; and that the time scale for complete evaporation of the companion is almost certainly greater than 10^7 yr. Our measurements are not easily accommodated by any of the proposed eclipse mechanisms, largely because of the observed dependence of eclipse duration upon frequency. If further observations show that the loss of pulsed

signal is not due to pulse smearing, a fresh look at possible mechanisms of eclipse may be required.

This work was carried out with financial assistance from the National Science Foundation, the National Bureau of Standards, the US Department of Education, the General Electric Foundation, and the State of New Jersey. We thank F. C. Michel, B. Paczyński, E. S. Phinney, F. Rasio, S. L. Shapiro, and A. C. Thompson for helpful discussions, and A. Wolszczan for sharing some observing time.

REFERENCES

Berman, G. 1989, Princeton University Physics Department, internal report.
Czerny, M., and King, A. R. 1988, *M.N.R.A.S.*, **235**, 33P.
Djorgovski, S., and Evans, C. R. 1988, *Ap. J. (Letters)*, **335**, L61.
Fruchter, A. S. 1989, Ph.D. thesis, Princeton University.
Fruchter, A. S., Gunn, J. G., Lauer, T. R., and Dressler, A. 1988, *Nature*, **334**, 686.
Fruchter, A. S., Stinebring, D. R., and Taylor, J. H. 1988, *Nature*, **333**, 237.
Hankins, T. H., and Rickett, B. J. 1975, *Meth. Comp. Phys.*, **14**, 55.
Hankins, T. H., and Stinebring, D. R. 1990, in preparation.
Hankins, T. H., Stinebring, D. R., and Rawley, L. A. 1987, *Ap. J.*, **315**, 149.
Kluźniak, W., Ruderman, M., Shaham, J., and Tavani, M. 1988, *Nature*, **334**, 225.
Kulkarni, S. R., Djorgovski, S., and Fruchter, A. S. 1988, *Nature*, **334**, 504.
Kulkarni, S. R., and Hester, J. J. 1988, *Nature*, **335**, 801.
Manchester, R. N., and Taylor, J. H. 1977, *Pulsars* (San Francisco: W. H. Freeman), Chap. 6.
Michel, F. C. 1989, *Nature*, **337**, 236.
Phinney, E. S., Evans, C. R., Blandford, R. D., and Kulkarni, S. R. 1988, *Nature*, **333**, 832.
Rasio, F., Shapiro, S., and Teukolsky, S. A. 1989, *Ap. J.*, **344**, 146.
Rawley, L. A., Taylor, J. H., and Davis, M. M. 1988, *Ap. J.*, **326**, 947.
Rawley, L. A., Taylor, J. H., Davis, M. M., and Allan, D. W. 1987, *Science*, **238**, 761.
Ryba, M. 1988, Princeton University Physics Department, internal report.
Ruderman, M., Shaham, J., and Tavani, M. 1989, *Ap. J.*, **336**, 507.
Stinebring, D. R., Bower, G., Fruchter, A. S., Klein, J. R., Ryba, M., Taylor, J. H., Thorsett, S. E., and Weisberg, J. M. 1989, in *Proc. 14th Symp. on Relativistic Astrophysics, Ann. NY Acad. Sci.*, in press.
Stinebring, D. R., and Cordes, J. M. 1983, *Nature*, **306**, 349.
Taylor, J. H., and Weisberg, J. M. 1989, *Ap. J.*, **345**, 434.
Thorsett, S. E. 1989, Princeton University Physics Department, internal report.
Thorsett, S. E., Fruchter, A. S., Stinebring, D. R., and Taylor, J. H. 1989, in *Proc. 14th Symp. on Relativistic Astrophysics, Ann. NY Acad. Sci.*, in press.
van den Heuvel, E. P. J., and van Paradijs, J. 1988, *Nature*, **334**, 227.
van Paradijs, J., *et al.* 1988, *Nature*, **334**, 684.
Wasserman, I., and Cordes, J. M. 1988, *Ap. J. (Letters)*, **333**, L91.

G. BERMAN, G. BOWER, M. CONVERY, J. R. KLEIN, D. J. NICE, M. F. RYBA, D. R. STINEBRING, J. H. TAYLOR, and S. E. THORSETT: Physics Department, Princeton University, Box 708, Princeton, NJ 08544

A. S. FRUCHTER: Department of Terrestrial Magnetism, Carnegie Institution of Washington, 5241 Broad Branch Road, N.W., Washington, DC 20015

W. M. GOSS: National Radio Astronomy Observatory, VLA, P.O. Box 0, Socorro, NM 87801

T. H. HANKINS: Department of Physics and Astronomy, New Mexico Institute of Mining and Technology, Socorro, NM 87801

J. M. WEISBERG: Department of Physics and Astronomy, Carleton College, Northfield, MN 55057